IET Renewable Power Generation

Special Issue Call for Papers

Be Seen. Be Cited.
Submit your work to a new IET special issue

Connect with researchers and experts in your field and share knowledge.

Be part of the latest research trends, faster.

Read more

The Institution of Engineering and Technology

Received: 10 December 2020 | Revised: 4 May 2021 | Accepted: 5 May 2021

IET Renewable Power Generation

DOI: 10.1049/rpg2.12208

The Institution of Engineering and Technology WILEY

ORIGINAL RESEARCH PAPER

Modelling and analysis of inertia self-tuning phase control strategy for a floating multi-body wave energy converter

Shaohui Yang[1,2,3] | Hu Chen[1,3] | Zhifei Ji[1,3] | Hui Li[1,3] | Xu Xiang[4]

[1] College of Mechanical and Energy Engineering, Jimei University, Xiamen, China

[2] Key Laboratory of Energy Cleaning Utilization and Development of Fujian Province, Xiamen, China

[3] Key Laboratory of Ocean Renewable Energy Equipment, Fujian Province University, Xiamen, China

[4] Norwegian Public Roads Administration, Complex constructions Brynsengfaret 6a, Oslo, Norway

Correspondence
Hu Chen, College of Mechanical and Energy Engineering, Jimei University, Xiamen City, Fujian Province, 361021, China.
Email: 13163996278g@163.com

Funding information
National Natural Science Foundation of China, Grant/Award Number: 51779104; Natural Science Foundation of Fujian Province, China, Grant/Award Number: 2020J01694; Foreign Cooperation Program of Fujian Province, China, Grant/Award Number: 2020I0021

Abstract

Wave energy converters (WECs) exhibit higher energy capture capacity when the wave frequency is close to the nature frequency of the device. A possible way to enhance energy capture efficiency is to modify the nature frequency of a WEC to match the incoming wave frequency. This paper presents an inertia self-tuning phase control strategy which can optimize the wave energy capture efficiency of a floating multi-body (FMB) WEC by regulating automatically the total mass of the capture energy part according to the incoming wave conditions. A variable-frequency inertia self-tuning control system is designed to conduct the proposed control strategy. The mathematical model of rotational motion of the FMB WEC is built and the dynamic performance of the control system is analysed in detail. Simulation results illustrate the proposed control strategy can achieve a phase optimization and hence significantly improve wave energy extraction of the FMB WEC in both regular and irregular waves. For regular waves, the maximum capture width ratio)CWR(under the control strategy is 7.3 times higher than that no control strategy is used. For irregular waves, the maximum CWR under the control strategy is 4.4 times that without the control strategy at the same wave frequency.

KEYWORDS

Inertia self-tuning, irregular wave, oscillating buoy, phase control, wave energy converter

1 | INTRODUCTION

Oceans cover two thirds of the earth's surface and large amount of ocean energy is contained within the motions of the waves. Energy extraction and conversion from ocean waves are now gaining more and more attention as the years pass by. With the increasing attention to harnessing the wave energy, many control and optimal technologies have been proposed and developed, aiming at increasing the wave energy conversion efficiency [1].

It is well-known that optimizing the geometric structure or shape of a WEC can achieve higher energy capture efficiency. A famous case is the nodding Duck WEC [2]. It was reported that the optimized hydrodynamic structure made the wave energy capture efficiency of the nodding Duck WEC reach 90% under ideal operating conditions [3]. The sharp eagle WEC proposed by the Guangzhou Institute of Energy conversion in China has an excellent wave energy absorbing capacity because the shape of the capturing energy buoy is designed to be like an eagle's beak [4, 5]. SEAREV WEC has been in development for many years in France. Three main generations of the technology have been defined and studied in detail since 2002. It has been proved that each new generation brought remarkable improvements over the previous generation because of the shape optimization [6]. Goggins and Finnegan [7] investigated the effects about optimizing the draft and the diameter of a double-body point absorbing WEC. The results showed that the optimization of the geometry parameters could clearly help to maximize the WEC's efficiency when considering specific wave conditions.

The purpose of optimization design is for matching the nature frequency of a WEC with the incoming wave frequency [8], that is the WEC should operate at the optimal phase condition (resonance condition) for improving wave energy capture capacity. When the optimal phase condition is satisfied, the heave motion velocity of the capture energy part is in phase with the wave excitation force. However, as real waves are not single-frequency and always vary with the time, the static shape and geometry optimization generally taking place in the design and manufacturing stage may get low energy conversion efficiency under the real sea conditions. Advanced dynamic control technologies must be employed to realize the automatic tuning of the WEC's nature frequency according to the sea states. Many phase control technologies for achieving optimal phase condition have been proposed and studied widely since 1970s [1, 9].

Latching control is one of the phase control technologies. It has been validated by some numerical analyses and physical experiments [10, 11]. In the latching control strategy, the control unit latches the capture energy device when its motion velocity reaches zero or is very small. In the process, the WEC will be halted for a certain period (i.e. the latching duration). When the WEC is released at the instant of de-latching, it is supposed to heave, and the heaving velocity is in-phase with the wave excitation force [10]. How to decide the latching duration is considered to be one of the challenges due to the requirement of detailed future wave information [12]. Another challenge for latching control strategy is the design of a mechanism or method to carry out the latching [13]. Besides, the optimal phase condition just is partially fulfilled in the latching control. Thus, latching control is often called the sub-optimal control [10, 14].

For satisfying the full phase control, the WECs must have the ability to regulate the internal dynamic parameters such as the elastic coefficient, the wet surface area or the inertia term of the WECs. In [15], a reactive control strategy has been proposed which can adjust the Power Take-off (PTO) elastic coefficient to counteract the intrinsic reactance of the WEC. In the reactive control strategy, a part of the extracted energy must be effectively fed back into the waves through the PTO and the elastic coefficient of the PTO must take negative value [8]. Tuning the wetted surface area can also fulfil phase optimum because the hydrodynamic elastic coefficient of the energy absorber is changed with the incident waves. As indicated in [16], the wetted surface area of an oscillating surge WEC is modified according to the real-time the sea states. That matches the natural period of the device with the peak excitation period of the sea spectrum to improve energy conversion efficiency. In [17], a mechanical controller is designed to tune the buoy-shaft titling angle so that the wet surface of hemispherical buoy can be adjusted. The flume experimental results indicate that the overall efficiency of the system can be improved by 15%.

Another approach utilized to satisfy the optimal phase condition is to tune the inertia of the WEC. In [18], the energy capture of a bottom-hinged pitching point absorber is improved by modifying the inertia of the device. The experimental results show that this method of inertia modification could result in an increase of capture factor by 70–100% for larger regular waves when compared to a constant inertia configuration. An analytical phase optimal procedure is presented for a double-body point absorbing WEC in [19]. Through invoking resonant conditions in the wave energy device, the authors illustrate how the phase optimal method has significant influence on the power capture characteristics of the WEC device. In [20], a fully submerged mass is added to a point-absorption WEC to properly shift the device's heave natural frequency and gain resonance with the most energetic waves to maximize the energy absorption. In [21], the inertia of a floating absorber is regulated for satisfying the optimal phase condition by changing the position of a sliding mass on the lever arm. The amount of extracted energy from the controlled system increases from about 1.1 to 2.9 times in irregular waves.

In this study, a novel inertia self-tuning phase control technology is proposed for maximizing the wave energy absorption of the FMB WEC which was validated by the numerical model and the real sea test in the previous works [22, 23]. A close-loop phase controller is designed to adjust the inertia of the energy capture part according to the sea states. The natural frequency of the FMB WEC is then altered and reaches automatically a value closer to the frequency of the incident wave so that the phase condition is satisfied. Simulation results in regular and irregular waves illustrate the performance and feasibility of the proposed control strategy.

2 | CONCEPT OF THE FMB WEC

Figure 1 shows the schematic of the FMB WEC which mainly consists of a floating platform, multiple oscillating buoys, actuating arms and PTOs. As shown in Figure 1, the oscillating buoys are distributed symmetrically around the floating platform and are linked with the floating platform through the actuating arms. For each actuating arm, there are three hinge axes designated as A, B and C, respectively. The hinge axis A allows rotation of the oscillating buoy respect with the floating platform; the hinge axis B links the PTO to the actuating arm and permits relative rotation of its anchor points, keeping the PTO perpendicular to the actuating arm; the hinge axis C joins the PTO to the supporting frame fixed on the floating platform. A damping plate is mounted under the floating platform. Under the operating mode, the damping plate is submerged into the seawater, reducing the heave amplitude of the floating platform and improving the stability of the whole system. Due to the wave forces, the relative heave motion between the oscillating buoy and the floating platform compresses or stretches the PTO on the actuating arm, thus converting wave energy to hydraulic energy.

A hydrodynamic mathematical model of the FMB WEC was built in [22]. Numerical analysis indicates that the dynamical property and energy conversion efficiency of the FMB WEC are related not only to the sea states but also to the geometric dimensions and the PTO coefficients of the FMB WEC. In [23], a 10 kW sea test prototype was developed and manufactured using a grant from the State Ocean Administration of China. A three-month real sea trial was carried out in the

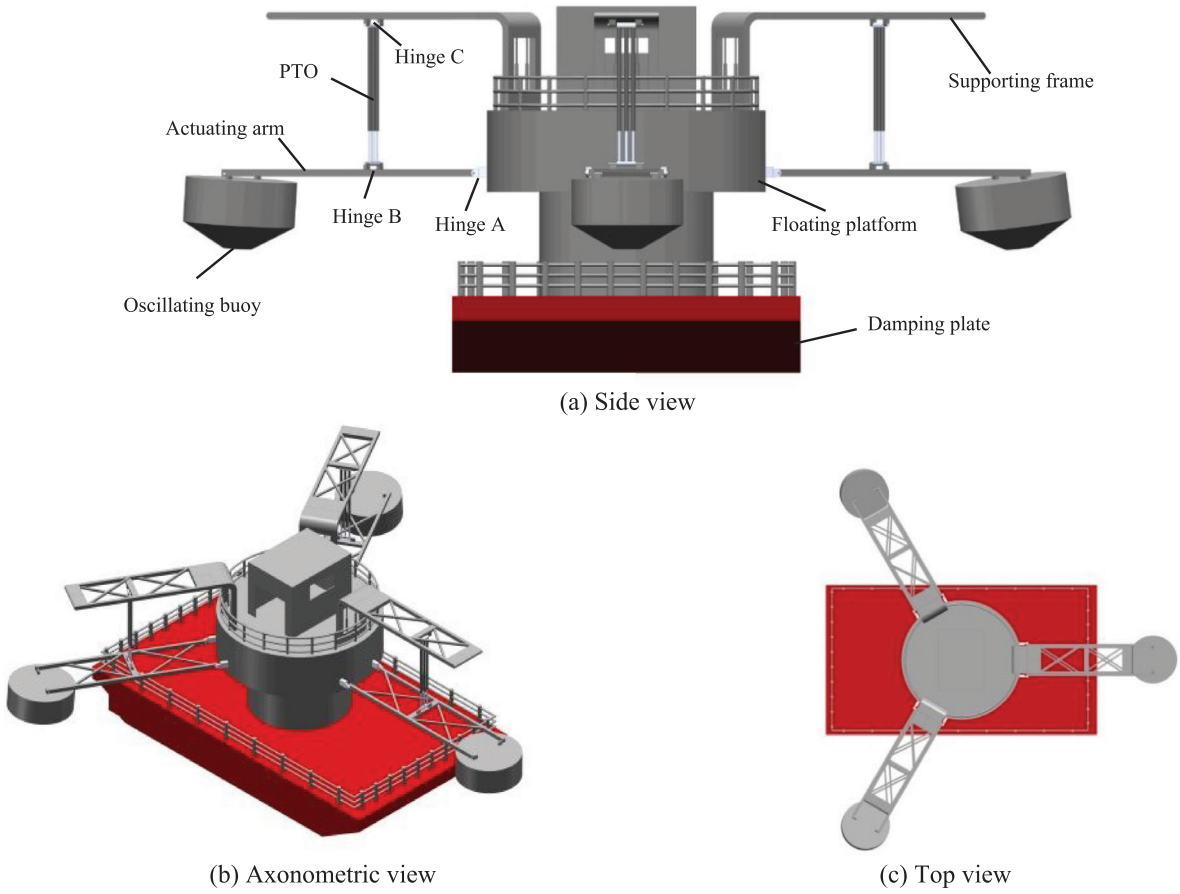

FIGURE 1 Schematic of the FMB WEC. (a) Side view. (b) Axonometric view. (c) Top view

Taiwan Strait, China. The experimental results confirmed that the FMB WEC had higher energy capture capacity when the wave periods were 3–5 s and the significant wave heights were 0.6–1.3 m. The increase in number of oscillating buoys used around the floating platform can increase the absorption of wave energy and improve the power output quality. Both the numerical analysis and sea test results proved that the heave amplitude of the floating platform is much less than the oscillating buoys because of their differences such as the hydrodynamic coefficient, mass property, geometric shape and so on. Therefore, in this study we assume that the floating platform is motionless for simplifying the analysis of the proposed control strategy. Figure 2 shows the prototype of the FMB WEC in real sea condition. Figure 2(a) is off-working state, Figure 2(b) is working state.

3 | MATHEMATICAL MODELING OF THE FMB WEC

According to the theory of fixed-point rotation for rigid bodies, the equilibrium equation of the moments around the hinge axis A of the FMB WEC can be expressed as:

$$J\ddot{\theta} = T_{hyd} - T_{pto} \tag{1}$$

where J is the moment of inertia, $J = mL^2$, m is the mass of each oscillating buoy, L is the length of each actuating arm; θ is the rotation angle displacement of the actuating arm; T_{hyd} is the hydrodynamic torque, $T_{hyd} = F_{hyd}L$, F_{hyd} refers to the hydrodynamic force produced by the incoming wave; T_{pto} is the PTO torque, $T_{pto} = F_{pto}L_1$, F_{pto} is the force produced by the PTO; L_1 is the distance between the hinge A and the PTO.

The hydrodynamic force, F_{hyd}, can be calculated as [15],

$$F_{hyd} = F_e - F_r - F_b \tag{2}$$

where F_e is the wave excitation force (due to the incident waves), F_r is the wave radiation force (due to the buoy's motion) and F_b is the hydrostatic restoring force (connected with the instantaneous position of the buoy with respect to the undisturbed free surface) [8].

F_r can be decomposed into components in phase with the buoy's acceleration and velocity [8, 15] so that

$$F_r = m_a\ddot{x} + c_w\dot{x} \tag{3}$$

where x is the heave displacement of the buoy, m_a is the added mass coefficient and c_w is the radiation damping coefficient. Both the added mass coefficient and the radiation damping

(a) Off-working state (b) Working state

FIGURE 2 Prototype of FMB WEC in real sea condition. (a) Off-working state. (b) Working state

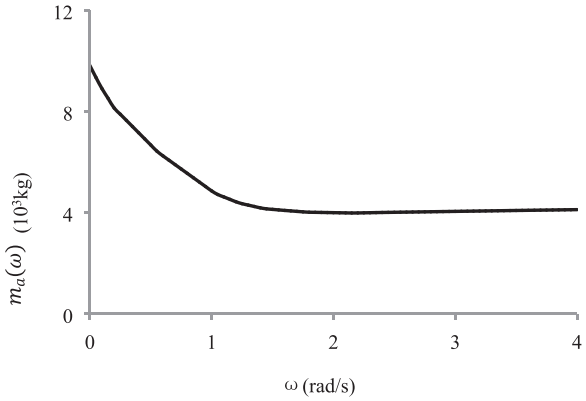

FIGURE 3 Added mass coefficient of the buoy

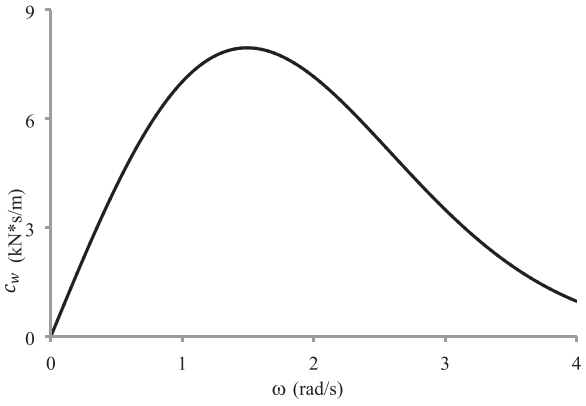

FIGURE 4 Radiation damping coefficient of the buoy

coefficient are the functions of the incident wave frequency [10, 15]. As shown in Figures 3 and 4, it can be seen that the buoy has a minimum added mass at wave frequency $\omega = 1.96$ rad/s, and its added mass approached a constant value at large frequencies. The radiation damping coefficient has a peak value at $\omega = 1.51$ rad/s. After reaching the peak value, the radiation coefficient begins to decrease as the wave frequency increasing.

When the heave motion of the buoy is small, that means the angle displacement θ of the actuating arm is small [28], so that

$$x \approx L\theta \tag{4}$$

Substituting Equation (4) into Equation (3), we can get

$$F_r = m_a L\ddot{\theta} + c_w L\dot{\theta} \tag{5}$$

And the hydrostatic restoring force F_b can be calculated as [15],

$$F_b = \rho g A_w x = \rho g A_w L\theta \tag{6}$$

Where ρ is the seawater density, g is the acceleration due to gravity, A_w is the cross-sectional area of the buoy by the unperturbed free surface plane, $A_w = \pi R_b^2$, R_b is the radius of each buoy.

If a full linear PTO is applied in further analysis, the PTO force can be expressed as:

$$F_{pto} = F_c + F_s \tag{7}$$

where F_c is the PTO damping force and F_s is the PTO elastic force which are proportional to the velocity and the displacement of the buoy, respectively [24]. The expressions are:

$$F_c = c_p \frac{L_1}{L} \dot{x} = c_p L_1 \dot{\theta} \tag{8}$$

$$F_s = k\frac{L_1}{L} x = kL_1\theta \tag{9}$$

where c_p and k is the PTO damping coefficient and elastic coefficient, respectively.

Substituting Equation (2), (5)–(9) into Equations (1), the equilibrium equation of the moments becomes:

$$mL^2\,\ddot{\theta} = F_e\,L - m_a L^2\ddot{\theta} - c_w L^2\dot{\theta} - \rho g A_w L^2\theta - c_p {L_1}^2\dot{\theta} - k{L_1}^2\theta \tag{10}$$

The corresponding frequency-domain equation of Equation (10) has a form as

$$\left[-\omega^2(m+m_a) + i\omega\left(c_w + c_p\left(\frac{L_1}{L}\right)^2\right) + \left(\rho g A_w + k\left(\frac{L_1}{L}\right)^2\right)\right]\theta\ (i\omega) = \frac{F_e(i\omega)}{L} \tag{11}$$

where ω is the incoming wave frequency. According to Equation (11), the solution of the angle displacement of the actuating arm can be obtained as:

$$\theta(i\omega) = \frac{F_e(i\omega)/L}{[\rho g A_w + k(L_1/L)^2] - \omega^2(m+m_a) + i\omega[c_w + c_p(L_1/L)^2]} \tag{12}$$

Equation (12) can be also re-written in terms of angle velocity,

$$V(i\omega) = \frac{F_e(i\omega)/L}{i\omega(m+m_a) + [c_w + c_p(L_1/L)^2] + [\rho g A_w + k(L_1/L)^2]/i\omega} \tag{13}$$

Looking at the transfer of power in the FMB WEC, the time averaged power captured by the PTO is calculated as:

$$\bar{P} = \frac{1}{2}\,c_p\left|L_1\overline{V\,(i\omega)}\right|^2 \tag{14}$$

The average capture power can be obtained in the analytical form as:

$$\bar{P} = \frac{1}{2}\,\frac{c_p L_1^2 |F_e(i\omega)|^2}{[c_w + c_p(L_1/L)^2]^2 + [\omega(m+m_a) - (\rho g A_w + k(L_1/L)^2)/\omega]^2} \tag{15}$$

where $|F_e(i\omega)|$ is the module of the wave excitation force.

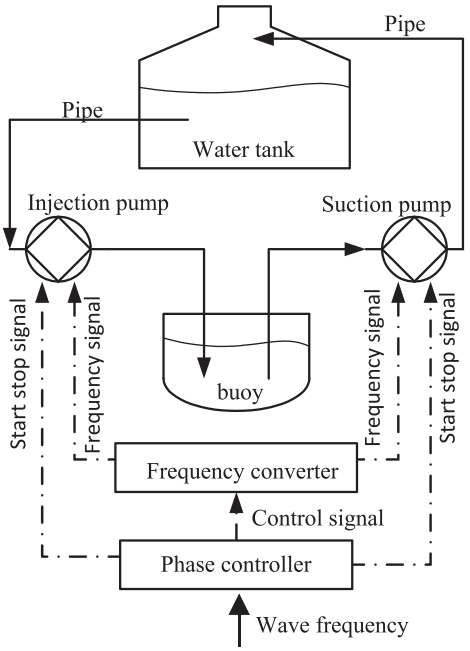

FIGURE 5 Structure diagram of the inertia self-tuning control system

From the look of the Equation (15), there exists a maximum value of the average captured energy if:

$$\omega(m+m_a) - \frac{(\rho g A_w + k(L_1/L)^2)}{\omega} = 0 \tag{16}$$

According to Equation (16), the nature frequency ω_n of the FMB WEC can be obtained as:

$$\omega_n = \sqrt{\frac{\rho g A_w + k\left(\frac{L_1}{L}\right)^2}{(m+m_a)}} \tag{17}$$

It is obvious that the angular velocity of the actuating arm is in phase with the wave excitation force and the optimal phase condition is satisfied when the incident wave frequency equals to the nature frequency of the FMB WEC. At the same time, it can be found we can change the mass of each buoy to ensure Equation (16) when the incident wave frequency varies.

4 | DESCRIPTION OF THE INERTIA SELF-TUNING CONTROL STRATEGY

4.1 | Control system structure

Figure 5 shows the structure of the proposed inertia self-tuning control system which is composed of a close-loop phase controller, a frequency converter, a variable-frequency injection pump, a variable-frequency suction pump and a water tank. It should be noticed that the altitude difference between the water

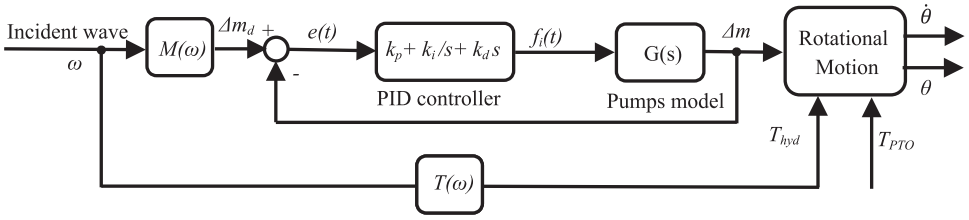

FIGURE 6 Block diagram of the close-loop phase controller. *M(ω)* represents the function relationship between Δm_d and ω. *T(ω)* represents the function relationship between the T_{hyd} and ω

tank and the buoys is about 7 m. According to the incoming wave frequency, the close-loop phase controller gives the control signal to change the inertia (i.e. the mass) of the oscillating buoy. For increasing the inertia, the injection pump is started and the fresh water in the water tanker is filled into the oscillating buoy. For decreasing the inertia, the suction pump is started and the fresh water is discharged from the oscillating buoy and returns to the water tank. The frequency converter gives the corresponding frequency signal to adjust the rotate speed of the variable-frequency pumps so that the water flow rate in the pipes can be controlled by the control system.

4.2 | Desired increment of the buoy mass

Since the total mass of each oscillating buoy is controlled to achieve the optimal phase condition, the corresponding nature frequency of the FMB WEC will vary with the buoy mass. The relation between the new nature frequency of the WEC and the increment of the buoy mass can be described as:

$$\omega_n' = \sqrt{\frac{\rho g A_w + k\left(\frac{L_1}{L}\right)^2}{(m + \Delta m + m_a)}} \tag{18}$$

where Δm represents the increment of the buoy mass. According to Equation (18), when the incident wave frequency is ω, the desired increment of the mass Δm_d should be:

$$\Delta m_d = \frac{\rho g A_w + k\left(\frac{L_1}{L}\right)^2}{\omega^2} - m - m_a \tag{19}$$

The mass of the buoy itself, m, is constant and its added mass, m_a, is frequency-dependent. Therefore, according to Equation (19), the desired increment of the buoy mass can be obtained if the incident wave frequency is given.

4.3 | Close-loop phase controller

In the inertia self-tuning control system, a close-loop phase controller is used to obtain the input frequency signal of the variable-frequency pumps according to the incident wave conditions. Figure 6 is the block diagram of the phase controller. It is assumed that the incident wave frequency has been measured and the desired value of Δm_d is determined according to Equation (19). Then, an error signal $e(t)$ is defined as the difference between the actual Δm and the desired Δm_d, and the input frequency signal $f_i(t)$ obtained by a proportional integral differentiation (PID) controller is sent to the injection/suction pumps. The pumps tune the total mass of the oscillating buoy by water suction or water drainage which consequently matches the natural frequency of the FMB WEC with the incoming wave frequency. The adjustment of the proportional gains k_p, the integral gain k_i and the differential gain k_d is based on pole placement method [25].

4.4 | Mathematical model of the pumps

The mathematical models of the injection pump and the suction pump are built as a second order transfer function.

$$G(s) = \frac{\Delta M(s)}{F_i(s)} = \frac{k_1}{s(Ts+1)} \tag{20}$$

where $\Delta M(s)$ and $F_i(s)$ are the Laplace transforms of the increment of the buoy mass and the pumps' input frequency signal, respectively. k_1 is the scale factor and T is the time constant. The instantaneous power P_c consumed by the pumps can be calculated as:

$$P_c = \frac{f_i^3}{f_r^3} P_r \tag{21}$$

where f_i is the input frequency of the pumps, f_r and P_r are the rated input frequency and rated power of the pumps, respectively.

5 | RESULTS AND ANALYSIS

In this section, the dynamic performances of the inertia self-tuning phase control strategy are investigated in regular and irregular wave conditions. The related hydrodynamic coefficients of the FMB WEC used in the simulation analysis are obtained via ANSIS AQWA software. Tables 1–4 show the values of the other related parameters. In the hydrodynamic numerical calculation, the geometry of the FMB WEC model is

TABLE 1 Geometrical parameters of the FMB WEC

Dimension parameters	Value
Radius of each buoy, R_b	1.6 m
Height of each buoy, H_b	2.2 m
Draft of each buoy, D_b	1.0 m
Radius of floating platform, R_b	4.0 m
Radius of damping plate, R_d	7.6 m
Depth of damping plate from still water level, D_s	6.0 m
Length of each actuating arm, L	6.8 m
Distance between the hinge A and the PTO, L_1	3.4 m

TABLE 2 PTO parameters used in the simulation

PTO Parameters	Value
Mass of each buoy, m	2000 kg
PTO damping coefficient, c_p	28 kN/(m/s)
PTO elastic coefficient, k	3.0 kN/ m

divided into meshes, as shown in Figure 7. The sea state parameters are set to the water depth of 15 m and the sea area of 100 m^2. The maximum grid size of the central platform and the buoys are 0.6 and 0.2 m, respectively. Meanwhile, the control strategy of the close-loop phase controller and the mathematical models of the pumps were analysed in the Matlab Simulink software. These hydrodynamic coefficients obtaining from the AQWA software are used in the programming codes of Matlab.

5.1 | Variation of buoy mass

Due to the limitation of the internal volume of the buoy, the maximum mass of the fresh water that can be filled into the buoy is about 18.0t. Therefore, the variation range of the total mass of each buoy is from 2.0t (the mass of each buoy itself) to 20.0t. Figure 8 depicts the relation between the desired increment of the mass and the incident wave frequency when the initial value of the buoy mass is set to 11.0t (i.e. 9.0t fresh water is filled into the buoy in the initial state). As shown in Figure 8, Δm_d decreases as the increase of the incident wave frequency when the incident wave frequency is between 1.78 and 3.62 rad/s. When the wave frequency is less than 2.32 rad/s, Δm_d is positive number that means the water in the water tank needs to be filled into the buoy. And when the wave frequency is larger than 2.32 rad/s, Δm_d is negative number that means the water needs to be discharged from the buoy. If the wave frequency is less than 1.78 rad/s, Δm_d is constant and equals to 9.0t. In this case, the total mass of the buoy is maximized and always equals to 20.0t. If the wave frequency is larger than 3.62 rad/s, Δm_d equals to −9.0t. The total mass of the buoy is minimized and always equals to 2.0t.

TABLE 3 Pumps parameters used in the simulation

Pumps parameters	Value
scale factor, k_1	3.33
Time constant, T	0.5s
Rated frequency, f_r	50 Hz
Rated power, P_r	7.5 kW
Rated displacement, V_r	72m^3/h
Rated speed, P_r	2900 rpm

TABLE 4 PID controller parameters used in the simulation

Controller parameters	Value
proportional gain, k_p	1.2
integral gain, k_i	0.001
differential gain, k_d	40

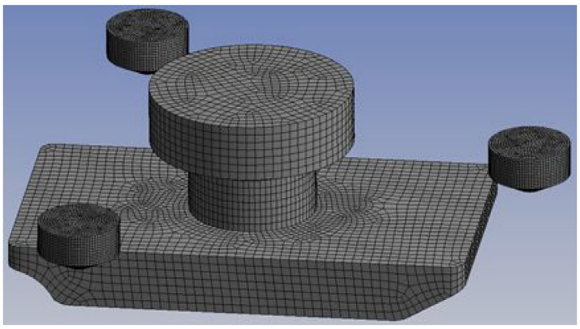

FIGURE 7 Hydrodynamic model of the FMB WEC

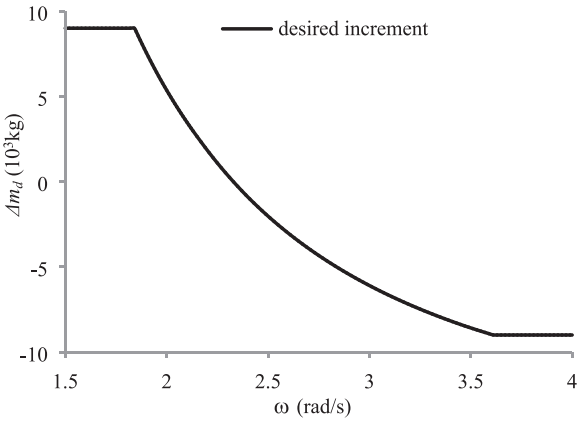

FIGURE 8 Relation curve between the desired increment of the buoy mass and the incident wave frequency

5.2 | Regular and irregular waves

In the study, a regular wave with a wave height of $H = 1.0$ m and a frequency of $\omega = 2.1$ rad/s is adopted to analyse the dynamic performance of the proposed control strategy as illustrated in Figure 10(a). For irregular wave, it can be represented

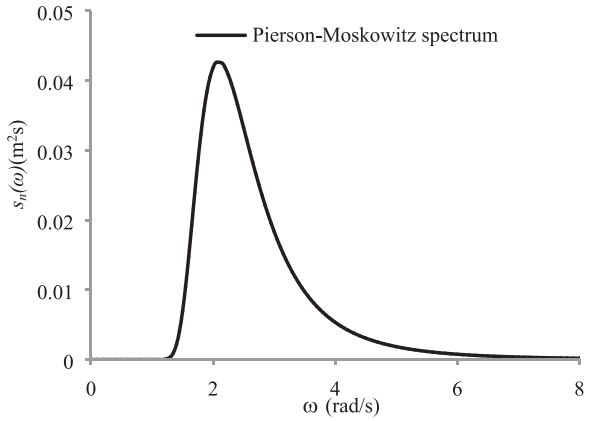

FIGURE 9 Pierson–Moskowitz wave spectrum when the significant wave height is 1.0 m and peak frequency is 2.1 rad/s

as a superposition of a set of regular waves. A conventional method is to describe an irregular wave by the wave spectrum with the corresponding significant wave height and peak period. The wave spectrum is a statistical feature in describing the distribution of the wave components. The conventional wave spectra used for wave energy extraction generally include the Pierson–Moskowitz spectrum, the Bretschneider spectrum and the JONSWAP spectrum. In this paper, we utilizes the Pierson–Moskowitz spectrum to describe the irregular wave which is defined as [26]:

$$S_n(\omega) = 5\pi^4 \frac{H_s^2}{T_p^4 \omega^5} \exp\left(-\frac{20\pi^4}{4T_p^4 \omega^4}\right) \tag{22}$$

with $\omega_p = 2\pi/T_p$, where T_p is the peak period, ω_p is the peak frequency and H_s is the significant wave height.

From the wave spectrum, a finite number of sinusoidal waves can be created. Each individual wave component is created with its own amplitude and frequency characterized by the spectrum. Each sinusoidal wave is assigned with a random phase and the wave elevation time series is generated as a sum of the individual components according to:

$$\eta(t) = \sum_{i=1}^{n} \sqrt{2 s_n(\omega_i) \Delta\omega} \sin(\omega_i t + \varphi_i) \tag{23}$$

where ω_i and φ_i are the frequency and random phase component of the ith wave, and $\Delta\omega$ is the frequency band calculated from:

$$\Delta\omega = \frac{\omega_{max}}{n} \tag{24}$$

where ω_{max} is the maximum frequency of the spectrum and n is the number of wave components. Figure 9 presents an example of a Pierson–Moskowitz spectrum and the corresponding H_s and ω_p are set as 1 m and 2.1 rad/s for the comparison with the regular wave in the following analysis. Figure 10(b) is the wave elevation time series of the irregular wave when $H_s = 1.0$ m and $\omega_p = 2.1$ rad/s.

5.3 | Dynamic performance in regular wave

Figure 11 shows the comparison of the angular displacements without and with the inertia self-tuning control strategy in the regular wave when $H = 1.0$ m and $\omega = 2.1$ rad/s. When no control strategy is applied to the FMB WEC, the angular displacement amplitude remains unchanged and is about 0.084. Under the control strategy, the angular displacement amplitude gradually increases with the simulation time and finally reaches to 0.126 as shown in Figure 11(b). The angular displacement amplitude has been significantly increased to about 1.5 times by the inertia self-tuning control strategy in the regular wave.

As shown in Figure 12, the power captured by the buoy with the control strategy also increases obviously when compared with the absorbed power by the uncontrolled buoy. As a result of the inertia self-tuning control strategy, the average capture power increases from 5.1 to 11.3 kW, an increase by 122%.

Figure 13 shows the variations of the input frequency of the injection pump and the power consumed by the injection pump for filling the water into the buoy. In the first 70 s of the simulation process, the input frequency and the consumed power equal to the rated frequency and the rated power of the injection pump, respectively. And then, the input frequency and the consumed power gradually decrease under the action of the phase controller. After about 140 s, the consumed power reduces to zero. As indicated in Figure 14, in accordance with the change of the consumed power of the pump, the increment of the buoy mass increases rapidly in the first 70 s. And at 140 s, the increment of the buoy mass reaches to the desired value, 3.41t, namely that the corresponding total mass of the buoy is 14.41t at this moment.

5.4 | Dynamic performance in irregular wave

One must note that the implementation of control strategies in irregular waves requires the prediction of the incoming waves. Nevertheless, the topic of wave prediction is beyond the scope of this paper. It is assumed that the sea state can be predicted for a specific time period in the near future. The power consumed by the pump and the desired increment of the buoy mass in irregular waves are calculated according to the peak frequency ω_p. When the peak frequency of the irregular wave is 2.1 rad/s, the variation tendencies of the control frequency, the consumed power of the pumps and the desired buoy mass increment are the same with that shown in Figures 13 and 14.

Figure 15 shows the comparison of angular displacement with and without control strategy in the irregular wave of $H_s = 1.0$ m and $\omega_p = 2.1$ rad/s. In the initial stage of the simulation, the angular displacements with and without control are roughly equal. In Figure 15(a), the average amplitude of the angular displacement is only 0.025 when no control strategy is applied in the FMB WEC. But under the control strategy, the angular displacement amplitude becomes larger with the increase of the total buoy mass as shown in Figure 15(b), and the average amplitude of the angular displacement reaches

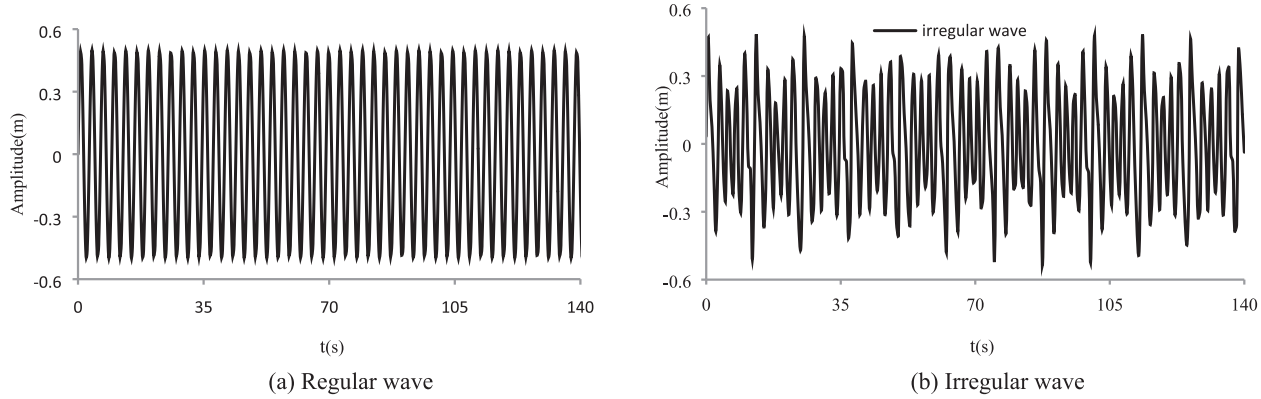

FIGURE 10 Comparison of regular wave and irregular wave of $H/H_s = 1.0$ m and $\omega/\omega_p = 2.1$ rad/. (a) Regular wave (b) Irregular wave

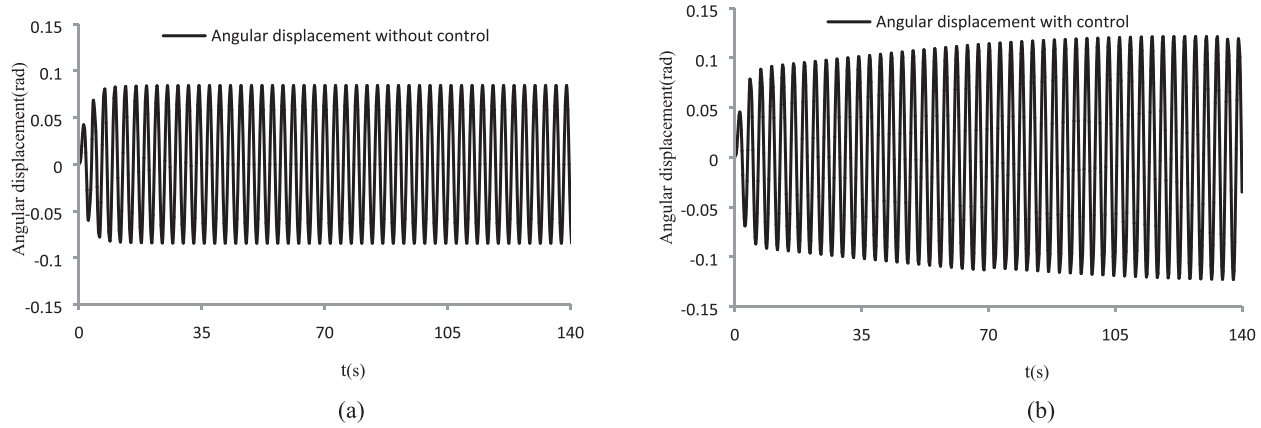

FIGURE 11 Comparison of angular displacements for inertia control to no control in a regular wave of $H = 1.0$ m and $\omega = 2.1$ rad/s. (a) Without control. (b) With control

to 0.038 when the increment of the buoy mass equals to the desired value.

Figure 16 shows the comparison of capture power with and without control strategy in the irregular wave of $H_s = 1.0$ m and $\omega_p = 2.1$ rad/s. It is very obvious that the absorbed power under the control strategy is larger than that without the control strategy. If the FMB WEC is left uncontrolled, the average capture power during the simulation process is 1.35 kW which is only 47% of the average capture power (2.86 kW) if the proposed control strategy is applied. The maximum instantaneous capture power without and with control are 5.43 and 11.07 kW, respectively.

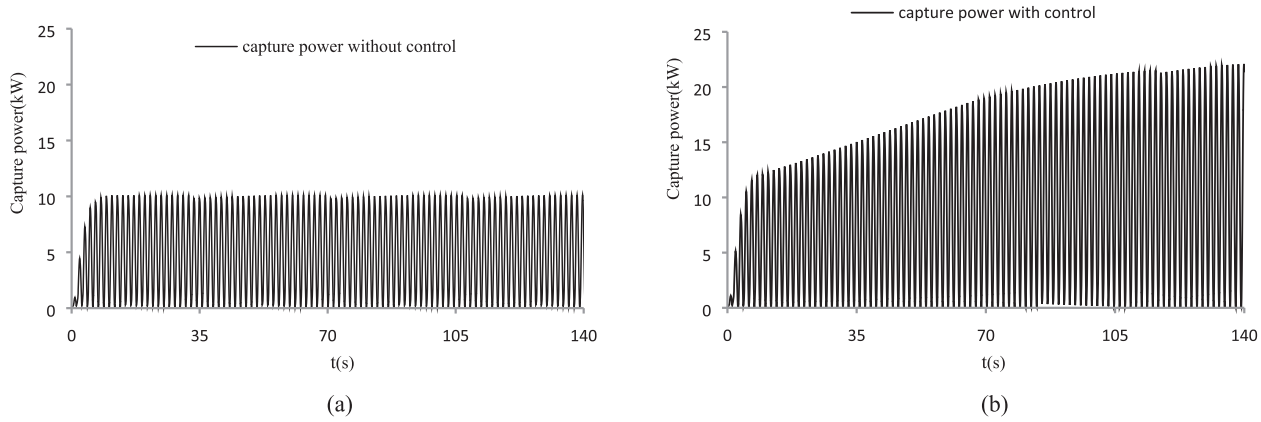

FIGURE 12 Comparison of capture power for inertia control to no control in a regular wave of $H = 1.0$ m and $\omega = 2.1$ rad/s. (a) Without control. (b) With control

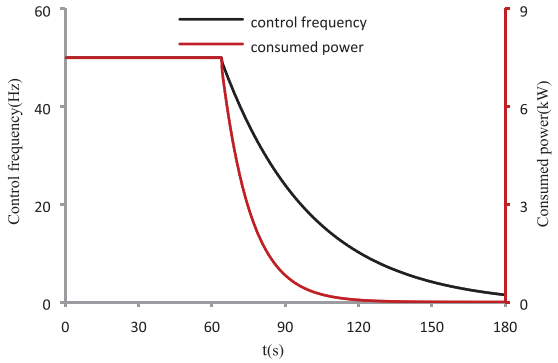

FIGURE 13 Variation curves of the control frequency and the power consumed by the injection pump when the incident wave frequency is 2.1 rad/s

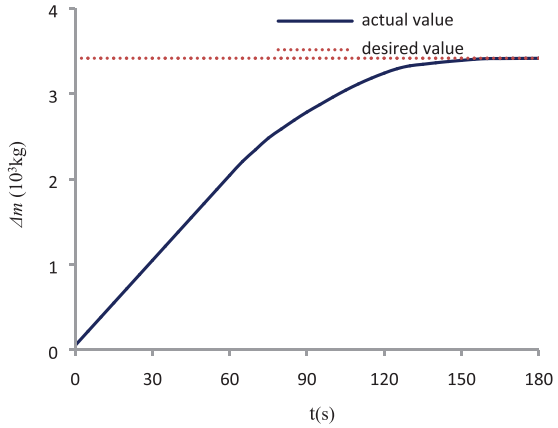

FIGURE 14 Comparison of desired and actual increment of the buoy mass with the inertia control strategy when the incident wave frequency is 2.1 rad/s

5.5 | Energy conversion efficiency

In this paper, the wave energy conversion efficiency is quantified in terms of capture width ratio (CWR) which is a key indicator utilized to estimate the energy capture capacity of a WEC [28]. In regular waves, the average wave power $\overline{P_r}$ per unit width can be calculated by this formula [15, 27]:

$$\overline{P_r} = \frac{\rho g^2}{32\pi} H^2 T \tag{24}$$

The CWR of the FMB WEC in regular waves can be defined as:

$$CWR = \frac{\bar{P}}{2R_b\overline{P_r}} \tag{25}$$

For irregular waves, the average wave power $\bar{P}_{ir}$ per unit width can be calculated by this formula [15, 26]:

$$\overline{P_{ir}} = \frac{\rho g^2}{64\pi} H_s^2 T_p \tag{26}$$

The CWR of the FMB WEC in irregular waves is:

$$CWR = \frac{\bar{P}}{2R_b\overline{P_{ir}}} \tag{27}$$

Figure 17 shows the comparison of CWRs at different wave frequencies without and with control strategy when the wave heights equal to 1 m. It can be seen the inertia self-tuning control strategy obviously enhances the CWRs and widens the response frequency band whether in regular waves or in irregular waves. If the FMB WEC is left uncontrolled, the maximum CWR is only 0.52 in regular waves and 0.27 in irregular waves. The wave frequency corresponding to the maximum CWR is 2.32 rad/s (i.e. the initial nature frequency). If the proposed control strategy is applied to the FMB WEC, the wave frequency corresponding to the maximum CWR shifts left to 1.78 rad/s and the maximum value of the CWRs rises to 3.14 in regular waves and 1.23 in irregular waves, respectively. For regular waves, the maximum CWR under the control strategy is 7.3 times higher than that no control strategy is used when $\omega = 1.78$ rad/s. However, for irregular waves, the maximum CWRs under the control strategy is 4.4 times that without the control strategy at the same wave frequency. It can be noted that the increase of the CWR is higher in regular waves than in irregular waves.

Figure 18 depicts the comparison between the extra energy extracted from the regular and irregular waves and the energy consumed by the pumps under the proposed control strategy when the wave heights are 1.0 m and the simulated time is set to 3600 s. The consumed energy equals to zero at the initial nature frequency (2.32 rad/s). But away from the initial nature frequency, the energy consumed by the control strategy increases on both sides for longer and shorter waves. When the incident wave frequency is greater than 3.5 rad/s or less than 1.8 rad/s, the consumed energy reaches the maximum value (3876 kJ). For the extra energy extracted from the waves under the control strategy, it can be seen that the proposed control strategy can extracted more energy in regular waves than in irregular waves. Take an example of a wave of $\omega/\omega_p = 1.8$ rad/s (wave height $H/H_s = 1.0$ m), the extra energy extracted from the regular wave is about 5.5 times that from the irregular wave. Moreover, it must be noted that the inertia self-tuning control strategy is more efficient in the lower wave frequencies (i.e. longer wave periods). When the wave frequency is greater than 2.4 rad/s, the consumed energy by the control strategy is more than the extra energy extracted from the waves because the wave energy per unit width is too small in such situation.

6 | CONCLUSIONS

In this study, an inertia self-tuning phase control strategy was proposed to increase the wave energy absorption of the FMB WEC. The proposed control strategy is based on the adjustment of the buoy mass to change the inertia of capture energy part. Then, the nature frequency of the FMB WEC reaches a value closer to the incident wave frequency and the phase

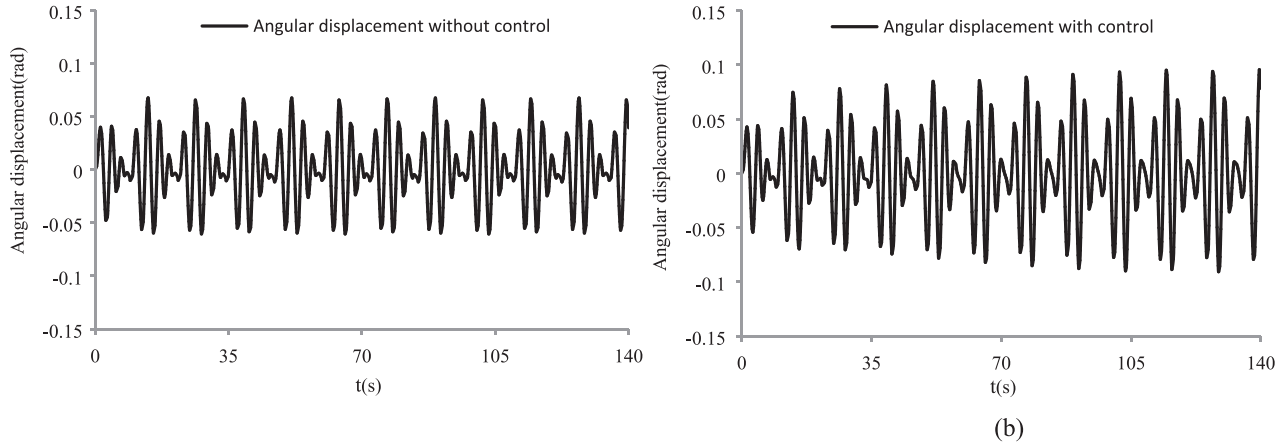

FIGURE 15 Comparison of angular displacements for inertia control to no control in an irregular wave of $H_s = 1.0$ m and $\omega_p = 2.1$ rad/s. (a) Without control. (b) With control

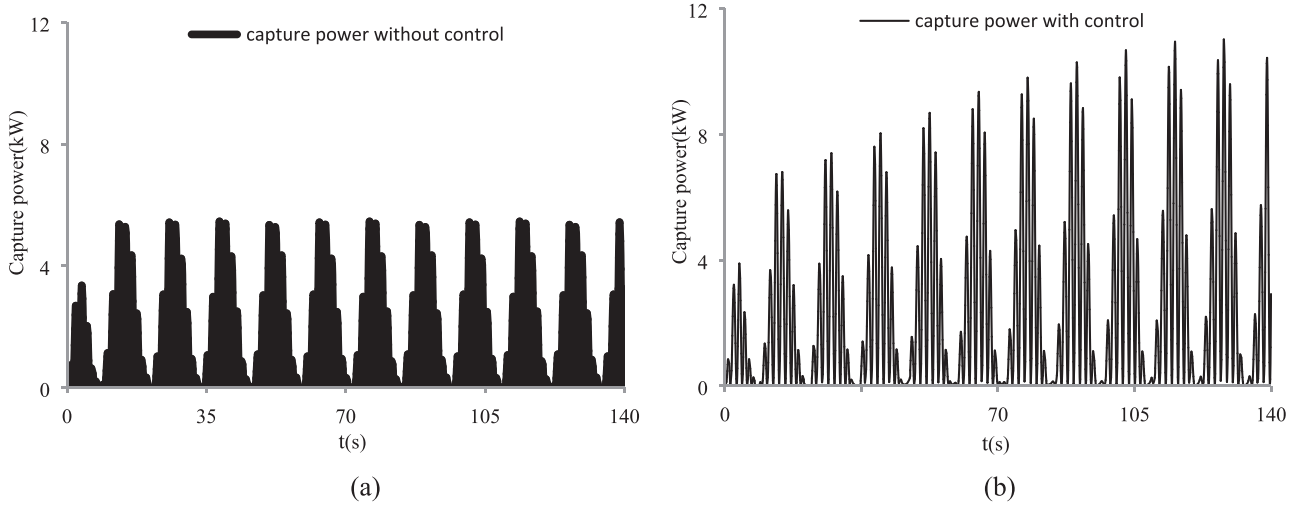

FIGURE 16 Comparison of the angular displacements for inertia control to no control in an irregular wave of $H_s = 1.0$ m and $\omega_p = 2.1$ rad/s. (a) Without control. (b) With control

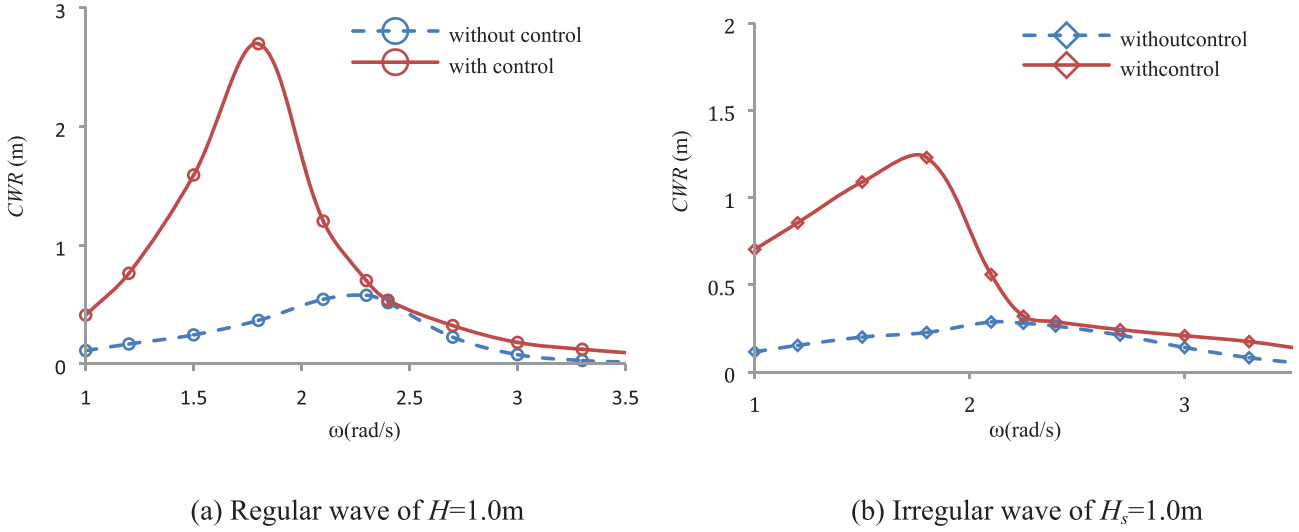

FIGURE 17 Comparison of the energy conversion efficiencies for inertia control to no control in regular and irregular waves for $H/H_s = 1.0$ m. (a) Regular wave of $H = 1.0$ m. (b) Irregular wave of $H = 1.0$ m.

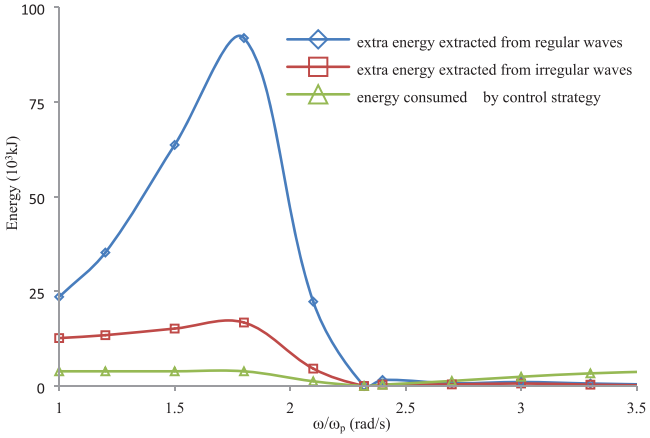

FIGURE 18 Comparison between extra energy extracted from regular and irregular waves under the control strategy and energy consumed by the control strategy when the simulated time is 3600 s

optimization condition is satisfied. An inertia control system and a phase controller were designed to perform the proposed control strategy.

The dynamic performance and energy conversion efficiency of the proposed control strategy were analysed for both regular and irregular waves. In the case of regular waves, the gain in the level of absorbed energy is higher, as the waves are characterized by a single frequency. Whether in regular waves or irregular waves, the proposed control strategy can improve significantly wave energy capture capacity of the FMB WEC. On the other hand, it should be noted that the proposed control strategy needs to consume some energy to change the inertia of the capture energy part. The consumed energy cannot be neglected especially when the wave frequency is very high.

ACKNOWLEDGMENTS

The authors would like to acknowledge the support of the National Natural Science Foundation of China (Grant No. 51779104), the Natural Science Foundation of Fujian Province, China (Grant Nos. 2020J01694) and the Foreign Cooperation Program of Fujian Province, China (Grant No. 2020I0021).

ORCID

Shaohui Yang https://orcid.org/0000-0002-7076-8598

REFERENCES

1. Hong, Y., Rafael, W., Cecilia, B.: Review on electrical control strategies for wave energy converting system. Renewable Sustainable Energy Rev. 31, 329–342 (2014)
2. Salter, S.H.: Wave power. Nature 249, 720–724 (1974)
3. Lin, Y., et al.: Review of hydraulic transmission technologies for wave power generation. Renewable Sustainable Energy Rev. 50, 194–203 (2015)
4. Sheng, S., et al.: Model research and open sea tests of 100kW wave energy convertor Sharp Eagle Wanshan. Renewable Energy 113, 587–595 (2017)
5. Zhang, Y., et al.: Study of hydrodynamic characteristics of a sharp eagle wave energy converter. China Ocean Eng. 31, 364–369 (2017)
6. Cordonnier, J., et al.: SEAREV: Case study of the development of a wave energy converter. Renewable Energy 80, 40–52 (2015)
7. Goggins, J., Finnegan, W.: Shape optimization of floating wave energy converters for a specified wave energy spectrum. Renewable Energy 71, 208–220 (2014)
8. António, F., Falcão, O.: Wave energy utilization: A review of the technologies. Renewable Sustainable Energy Rev. 14, 899–918 (2010)
9. Wang, L., Isberg, J., Tedeschi, E.: Review of control strategies for wave energy conversion systems and their validation: The wave-to-wire approach. Renewable Sustainable Energy Rev. 81, 366–379 (2018)
10. Sheng, W., Alcorm, R., Lewis, A.: On improving wave energy conersion, Part I: Optimal and control technologies. Renewable Energy 75, 922–934 (2015)
11. Babarit, A., Clement, A.H.: Optimal latching control of a wave energy device in regular and irregular waves. Appl. Ocean Res. 28, 77–91 (2006)
12. Hals, J., Falnes, J., Moan, T.: A comparison of selected strategies for adaptive control of wave energy converters. J. Offshore Mech. Arct. Eng. 33, 159–164 (2011)
13. Sheng, W., Alcorm, R., Lewis, A.: On improving wave energy conersion, Part II: Development of latching control technologies. Renewable Energy 75, 935–944 (2015)
14. Falcao, A.F.: Modelling and control of oscillating-body wave energy converters with hydraulic power take-off and gas accumulator. Ocean Eng 34, 2021–2032 (2007)
15. Falnes, J.: Ocean Waves and Oscillating Systems: Linear Interactions Including Wave Energy Extraction. Cambridge University Press, Cambridge. UK (2002)
16. Tom, N., Lawson, M., Yu, Y.H.: Spectral modeling of an oscillating surge wave energy converter with control surfaces. Appl. Ocean Res. 56, 143–156 (2016)
17. Do, H.T., et al.: Proposition and experiment of a sliding angle self-tuning wave energy converter. Ocean Eng. 132, 1–10 (2017)
18. Flocard, F., Finnigan, T.D.: Increasing power capture of a wave energy device by inertia adjustment. Appl. Ocean Res. 34, 126–134 (2012)
19. Bubbar, K., Buckham, B.: On establishing generalized analytical phase control conditions in two body self-reacting point absorber wave energy converters. Ocean Eng. 197, 106879 (2020)
20. Piscopo, V., Benassai, G., Cozzolino, L.: A new optimization procedure of heaving point absorber hydrodynamic performances. Ocean Eng. 116, 242–259 (2016)
21. Paulo, R., Paula, B., Segen, F.: Phase control strategy for a wave energy hyperbaric converter. Ocean Eng. 37, 1483–1490 (2010)
22. Yang, S.H., et al.: Dynamic properties and energy conversion efficiency of a floating multi-body wave energy converter. Chinese Ocean Eng. 32, 347–357 (2018)
23. Yang, S.H., et al.: Design and experiment research on array-raft wave energy power generation system. J. Mech. Eng. 52, 57–63 (2016)
24. Babarit, A., et al.: Numerical benchmarking study of a selection of wave energy converters. Renewable Energy 41, 44–63 (2012)
25. Russel, G.T.: A design methodology for nonlinear systems. Nonlinear Syst. Design 56, 129–144 (1984)
26. Cargo, C.J., Hillis, A.J., Plummer, A.R.: Optimisation and control of a hydraulic power take-off unit for a wave energy converter in irregular waves. J. Power Energy 228, 462–479 (2014)
27. Sheng, W., Lewis, A.: Assessment of wave energy exraction from seas: Numerical validation. J. Energy Res. Technol. 134, 146–154 (2012)
28. Babarit, A.: A database of capture width ratio of wave energy converters. Renewable Energy 80, 610–628 (2015)

How to cite this article: Yang S, Chen H, Ji Z, Li H, Xiang X. Modeling and analysis of inertia self-tuning phase control strategy for a floating multi-body wave energy converter. IET Renew. Power Gener.. 2021;15:3126–3137. https://doi.org/10.1049/rpg2.12208.